ORIGINAL RESEARCH • NEURORADIOLOGY

Radiology

Gadolinium Deposition in the Rat Brain Measured with Quantitative MRI versus Elemental Mass Spectrometry

Ning Hua, PhD • Olga Minaeva, PhD* • Nicola Lupoli, BS • Erich S. Franz, BS • Xiuping Liu, MD • Juliet A. Moncaster, PhD • Katharine J. Babcock, MS • Hernán Jara, PhD • Yorghos Tripodis, PhD • Ali Guermazi, MD, PhD • Jorge A. Soto, MD • Stephan W. Anderson, MD • Lee E. Goldstein, MD, PhD*

From the Departments of Radiology (N.H., O.M., N.L., X.L., J.A.M., H.J., A.G., J.A.S., S.W.A., L.E.G.), Neurology (L.E.G.), Pathology & Laboratory Medicine (L.E.G.), Anatomy & Neurobiology (K.J.B.), and Biostatistics (Y.T.), Boston University School of Medicine, 670 Albany St, 4th Floor, Boston, MA 02118; Boston University Alzheimer's Disease Research Center (N.H., O.M., J.A.M., L.E.G.), Boston, Mass; and Center for Biometallomics (O.M., N.L., J.A.M., L.E.G.), College of Engineering (E.S.F., S.W.A., L.E.G.), and Photonics Center (O.M., J.A.M., S.W.A., L.E.G.), Boston University, Boston, Mass. Received August 24, 2021; revision requested October 12; revision received June 8, 2022; accepted July 15. **Address correspondence to** L.E.G. (email: *lgold@bu.edu*).

Supported in part by GE Healthcare; in-kind support from Thermo Fisher Scientific. H.J. supported by National Institute of Neurological Disorders and Stroke (5U01NS040069-05 and 2R01NS040069-09), National Institutes of Health Office of the Director (5UH3OD023348-05), and National Institute of Child Health and Human Development (5P30HD018655-28).

* N.H. and O.M. contributed equally to this work.

Conflicts of interest are listed at the end of this article.

Radiology 2023; 306:244–251 • https://doi.org/10.1148/radiol.212171 • Content codes: NR MR

Background: T1-weighted MRI and quantitative longitudinal relaxation rate (R1) mapping have been used to evaluate gadolinium retention in the brain after gadolinium-based contrast agent (GBCA) administration. Whether MRI measures accurately reflect gadolinium regional distribution and concentration in the brain remains unclear.

Purpose: To compare gadolinium retention in rat forebrain measured with in vivo quantitative MRI R1 and ex vivo laser ablation inductively coupled plasma mass spectrometry (LA-ICP-MS) mapping after gadobenate, gadopentetate, gadodiamide, or gadobutrol administration.

Materials and Methods: Adult female Sprague-Dawley rats were randomly assigned to one of five groups (eight per group) and administered gadobenate, gadopentetate, gadodiamide, gadobutrol (2.4 mmol/kg per week for 5 weeks), or saline (4.8 mL/kg per week for 5 weeks). MRI R1 mapping was performed at baseline and 1 week after the final injection to determine R1 and ΔR1. Postmortem brains from the same rats were analyzed with LA-ICP-MS elemental mapping to determine regional gadolinium concentrations. Student *t* tests were performed to compare results between GBCA and saline groups.

Results: Rats that were administered gadobenate showed gadolinium-related MRI ΔR1 in 39.5% of brain volume (ΔR1 = 0.087 second^{-1} ± 0.051); gadopentetate, 20.6% (ΔR1 = 0.069 second^{-1} ± 0.018); gadodiamide, 5.4% (ΔR1 = 0.055 second^{-1} ± 0.019); and gadobutrol, 2.2% (ΔR1 = 0.052 second^{-1} ± 0.041). Agent-specific gadolinium-related ΔR1 was detected in multiple forebrain regions (neocortex, hippocampus, dentate gyrus, thalamus, and caudate-putamen) in rats treated with gadobenate or gadopentetate, whereas rats treated with gadodiamide showed gadolinium-related ΔR1 in caudate-putamen. By contrast, LA-ICP-MS elemental mapping showed a similar regional distribution pattern of heterogeneous retained gadolinium in the forebrain of rats treated with gadobenate, gadopentetate, or gadodiamide, with the average gadolinium concentration of 0.45 μg · g^{-1} ± 0.07, 0.50 μg · g^{-1} ± 0.10, and 0.60 μg · g^{-1} ± 0.11, respectively. Low levels (0.01 μg · g^{-1} ± 0.00) of retained gadolinium were detected in the forebrain of gadobutrol-treated rats.

Conclusion: Differences in in vivo MRI longitudinal relaxation rate versus ex vivo elemental mass spectrometry measures of retained gadolinium in rat forebrains suggest that some forms of retained gadolinium may escape detection with MRI.

Online supplemental material is available for this article.

Gadolinium-based contrast agents (GBCAs) are widely used in diagnostic MRI and have highly favorable safety profiles (1–3). However, emerging evidence suggests that repeated administration of GBCAs is associated with gadolinium retention in the brain, even in patients with normal renal function (4–9). Clinical reports of GBCA-associated gadolinium retention in gray matter nuclei (notably, dentate nucleus, globus pallidus, and thalamic nuclei) have been confirmed in laboratory animals after intravenous GBCA administration (10–15). In addition, nonhomogeneous gadolinium retention has been identified in specific regions of the cerebral cortex after GBCA administration in rats and humans (14). For example, rats administered gadopentetate dimeglumine showed regional, subregional, and layer-specific gadolinium retention in the anterior cingulate cortex and piriform cortex at tissue concentrations comparable to subcortical structures known to retain gadolinium (14).

T1-weighted MRI has been used to detect and monitor gadolinium retention in the human brain. Retained gadolinium increases the longitudinal relaxation rate (R1), which equals 1/T1, and produces hyperintensities detectable with T1-weighted MRI (16). Although T1-weighted MRI is a convenient method to assess gadolinium retention in vivo, this technique provides an indirect measure that is sensitive to local microenvironment factors that affect T1-weighted signals and interpretation. Moreover, T1-weighted MRI methods to assess gadolinium retention

Abbreviations

GBCA = gadolinium-based contrast agent, LA-ICP-MS = laser ablation inductively coupled plasma mass spectrometry

Summary

Gadolinium retention in the brain measured with MRI longitudinal relaxation rate mapping and laser ablation inductively coupled plasma mass spectrometry yielded different results, indicating that some forms of retained gadolinium may escape detection with MRI.

Key Results

- Gadolinium retention in the rat brain after repeated gadolinium-based contrast agent administration was measured with MRI longitudinal relaxation rate (R1) mapping and mass spectrometry.
- With MRI R1 mapping, brain gadolinium retention was higher for gadobenate versus gadodiamide and gadobutrol ($P < .001$ for gadobenate or gadopentetate vs gadodiamide).
- With mass spectrometry, gadolinium retention was higher for gadodiamide (0.60 $\mu g \cdot g^{-1} \pm 0.11$) versus gadobenate (0.45 $\mu g \cdot g^{-1} \pm 0.07$) and gadobutrol (0.01 $\mu g \cdot g^{-1} \pm 0.00$) ($P < .01$ for trend).

require use of a reference tissue that can introduce systematic bias. By contrast, R1 mapping, a quantitative implementation of T1-weighted MRI, is not subject to these confounds. However, whether MRI R1 mapping accurately reflects gadolinium retention and distribution in the brain remains unclear. Understanding these relationships is critical for accurate interpretation of MRI measures of gadolinium retention in the brain.

Laser ablation inductively coupled plasma mass spectrometry (LA-ICP-MS) is a powerful technique that enables definitive identification, analytical quantitation, and high-resolution spatial mapping of elements and isotopes in biologic tissues (11,14,17,18). This technique is recognized as the analytical standard for elemental detection and mapping of gadolinium retention in the brain. In this study, we hypothesized that MRI R1 and LA-ICP-MS mapping would detect the same regionally distributed pools of retained gadolinium in the brain after GBCA administration. To evaluate this hypothesis, we compared in vivo quantitative R1 maps and ex vivo LA-ICP-MS maps of gadolinium retention in the forebrain of rats after repeated intravenous injection of one of four GBCAs or saline (the control).

MRI examinations with GBCAs are associated with gadolinium retention in the brain (4–13). However, the question of whether MRI results accurately reflect gadolinium concentrations and distribution in the brain remains unanswered. The aim of the study is to evaluate if MRI R1 mapping could accurately reflect gadolinium concentrations and distribution in the brain. The GBCAs investigated in this study are commercially available and commonly used for clinical MRI examinations. The representative GBCAs were chosen from different classes and varied by molecular structure, complex ionization, and thermodynamic stability.

Materials and Methods

Experimental Design and Animal Subjects

Female Sprague-Dawley rats ($n = 40$; Charles River Laboratories), 9–10 weeks of age, were group housed (Boston University Animal Science Center) and randomly assigned to one of four treatment groups (eight per group): gadobenate (MultiHance; Bracco Diagnostics), gadopentetate (Magnevist; Bayer Healthcare), gadodiamide (Omniscan; GE Healthcare), or gadobutrol (Gadovist; Bayer Healthcare) with one dose (2.4 mmol/kg, intravenous) per week for 5 weeks. The selected GBCAs differ by class and exhibit different thermodynamic stabilities according to the following rank order: macrocyclic nonionic (gadobutrol), linear ionic (gadobenate and gadopentetate), and linear nonionic (gadodiamide). A control group was treated with volume-matched saline (4.8 mL/kg per week for 5 weeks). GBCA dosing was harmonized with recent preclinical studies and represents four human-equivalent GBCA doses adjusted for total body surface area (14,19). MRI scans were acquired before the first (pre-exposure) and 1 week after the final (fifth) GBCA or saline injection (post-exposure). Rats were sacrificed within 3 hours after postexposure MRI examination by CO_2 asphyxiation and transcardial perfusion with 200-mL phosphate-buffered saline followed by 200-mL 4% (weight by volume) paraformaldehyde. Harvested brains were submerged in 4% paraformaldehyde for 24 hours, transferred to phosphate-buffered saline, and stored at 4°C. Brains were hemisected, cryoprotected in 30% sucrose (weight by volume) for 3 days, snap frozen in isopentane cooled in liquid nitrogen, and stored at −20°C until analysis. The study was approved by the Institutional Animal Care and Use Committee at Boston University.

MRI Acquisition and Quantitative R1 Analysis

Rat MRI (3.0-T Achieva; Philips) scans were acquired (N.H., with >15 years of experience) at both pre- and post-exposure time points (eight per group; 40 rats total). During MRI, rats were anesthetized with isoflurane (Butler Schein Animal Health) (induction, 3.5% vol/vol; maintenance, 1.5%–2% vol/vol) and inserted into a 16-element knee coil. A mixed turbo spin-echo sequence was used to obtain R1 maps with use of a quadruple time point sequence that combines R1 weighting by inversion recovery and transverse relaxation rate (hereafter, R2) weighting by multiecho sampling in a single acquisition. This sequence uses two inversion times and two effective echo times to generate four self-coregistered images per section, each with different R1 and R2 weighting. Four acquired images were processed to generate R1 and R2 maps. The key parameters for the images were as follows: inversion time, 1000 msec; repetition time of the inversion recovery portion, 4000 msec; repetition time of the spin echo portion, 3000 msec; echo times, 12.9 and 90 msec; field of view, 40 × 40 mm^2; acquisition matrix size, 100 × 96; in-plane resolution, 0.30 × 0.32 mm^2 reconstructed to 0.18 × 0.18 mm^2; section thickness, 2 mm; and number of averages, six. R1 maps were generated with use of in-house MATLAB (MathWorks, R2017b) software as previously described (20–22). The R1 histogram for each rat was modeled by using a bi-Gaussian fitting to obtain R1 of gray and white matter separately (23). A voxel-based method was used to assess regional differences. Skull-striped images were registered to a T2-weighted template (24) with use of the FMRIB Software Library *(https://fsl.fmrib.ox.ac.uk/fsl/fslwiki)* (25). Registered R1

Table 1: Averaged R1 Mapping MRI Values for Gray Matter and White Matter for Each Experimental Group of Rats

	Gray Matter R1*			White Matter R1*		
Treatment	$R1_{Pre}$	$R1_{Post}$	$\Delta R1$ ($\Delta R1_{Post}$–$R1_{Pre}$)	$R1_{Pre}$	$R1_{Post}$	$\Delta R1$ ($\Delta R1_{Post}$–$R1_{Pre}$)
Saline	1.042 ± 0.012	1.068 ± 0.013†	0.026 ± 0.014	1.234 ± 0.013	1.268 ± 0.018†	0.034 ± 0.011
Gadobutrol	1.044 ± 0.017	1.073 ± 0.017‡	0.029 ± 0.017	1.232 ± 0.025	1.267 ± 0.020§	0.035 ± 0.027
Gadodiamide	1.054 ± 0.027	1.092 ± 0.014†	0.038 ± 0.018	1.244 ± 0.034	1.281 ± 0.018‡	0.037 ± 0.021
Gadopentetate	1.026 ± 0.026	1.089 ± 0.008‡	0.063 ± 0.029	1.213 ± 0.033	1.279 ± 0.019‖	0.066 ± 0.038
Gadobenate	1.004 ± 0.042	1.087 ± 0.014†	0.083 ± 0.038	1.188 ± 0.044	1.274 ± 0.014‡	0.086 ± 0.045

Note.—Values represent means ± SDs. R1 = longitudinal relaxation rate, $R1_{Post}$ = R1 at the post-injection time point, $R1_{Pre}$ = R1 at the pre-injection time point, ΔR1 = R1 changes.

* Values are measured in $second^{-1}$.

† The *P* value significance level for pre- versus post-injection R1 values is $P < .001$.

‡ The *P* value significance level for pre- versus post-injection R1 values is $P = .001$.

§ The *P* value significance level for pre- versus post-injection R1 values is $P = .004$.

‖ The *P* value significance level for pre- versus post-injection R1 values is $P = .002$.

maps from prior (hereafter, $R1_{pre}$) and post (hereafter, $R1_{post}$) contrast material administration were used to calculate R1 changes ($\Delta R1 = R1_{post} - R1_{pre}$). To compensate for normal aging, ΔR1 maps for each GBCA group were compared with the saline group with use of voxel-by-voxel Student *t* tests. ΔR1 in voxels that were significantly different ($P < .05$) compared with the saline control group were considered related to GBCA treatment. Identified voxels were normalized to total brain volume (1.86 cm^3) in template space (24) to obtain percentage brain volume with gadolinium-related ΔR1.

LA-ICP-MS Elemental Brain Mapping

Elemental brain mapping (gadobenate, $n = 6$; gadopentetate, $n = 5$; gadodiamide, $n = 5$; gadobutrol, $n = 6$; saline, $n = 7$) was performed with LA-ICP-MS imaging (O.M., with >15 years of experience in imaging; N.L., with >25 years of experience in mass spectrometry) with use of a laser ablation system (LSX-213; Teledyne CETAC Technologies) hyphenated to a quadrupole inductively coupled plasma mass spectrometer (iCAP-Q; Thermo Fisher Scientific), as previously described (14). Analytical calibrations of gadolinium-LA-ICP-MS maps were conducted by using gadolinium-spiked gelatin standards (10% wt/vol) (17). The calibration curves had eight points (0.0–3.0 $\mu g \cdot g^{-1}$). Gadolinium 158 LA-ICP-MS maps were calibrated for total gadolinium concentration. Brain sections and standards were cryosectioned (CM1850; Leica Biosystems) at 10-μm thickness and scanned by using the following parameters: spot size = 50 μm, line separation = 0 μm, and scan speed = 100 μm · $second^{-1}$. LA-ICP-MS data were exported to a customized MATLAB program (MathWorks, R2017b) and ImageJ (NIH open-source software, version 2.1.0/1.53c) for quantitative analysis. Two readers (L.E.G., with >35 years of experience in experimental pathology, blinded to groups; N.H., with >15 years of experience in preclinical imaging) drew manual contours to calculate gadolinium concentrations in regions of interest based on the Paxinos and Watson atlas (26). Values were averaged for each GBCA group.

Statistical Analysis

The R1 and ΔR1 values of gray and white matter are presented as means ± SDs. Gadolinium concentration measured with LA-ICP-MS are reported as means ± standard errors of the means for each region of interest per treatment group. The intraclass correlation coefficient was calculated in SPSS (IBM, version 27) to assess the reliability of region-of-interest measurements. Student *t* tests were performed in MATLAB (MathWorks, R2017b) to compare each GBCA group to the saline group. To control for the family-wise error in ΔR1 mapping, a cluster-based permutation method was used. For all statistical tests, significance was defined as $P < .05$.

Results

Gadolinium Retention in Rat Brain Evaluated with Antemortem MRI R1 Mapping

Table 1 shows the average R1 values and ΔR1 for gray and white matter before and 1 week after the final (fifth) injection of GBCA or saline. Mean R1 values in gray and white matter at 1 week after the final (fifth) injection were significantly greater versus mean R1 values at baseline for all GBCA and saline groups (Table 1; all $P < .01$). The R1 increase observed in saline-treated rats is consistent with expected aging-related changes in myelination between MRI acquisitions. Therefore, we conducted a voxel-based analysis of the R1 values (Figs 1, E1 [online]) and compared results to the saline group to isolate regions that showed additional R1 increases attributable to the gadolinium exposure. Gadolinium-related R1 changes ($\Delta R1 = R1_{post} - R1_{pre}$) were overlaid on a T2-weighted MRI template (24) for anatomic visualization. Consistent with previous studies (10,11,13,14), we detected gadolinium-related R1 increases in deep cerebellar nuclei and pons of rats treated with gadodiamide, gadopentetate, or gadobenate (Fig E1 [online]). In the forebrain, ΔR1 showed agent-specific patterns of gadolinium-related changes.

In the gadobenate group, 39.5% (0.73 of 1.86 cm^3) of brain volume showed gadolinium-related ΔR1, and in those regions, average ΔR1 was 0.087 $second^{-1}$ ± 0.051. Bilateral

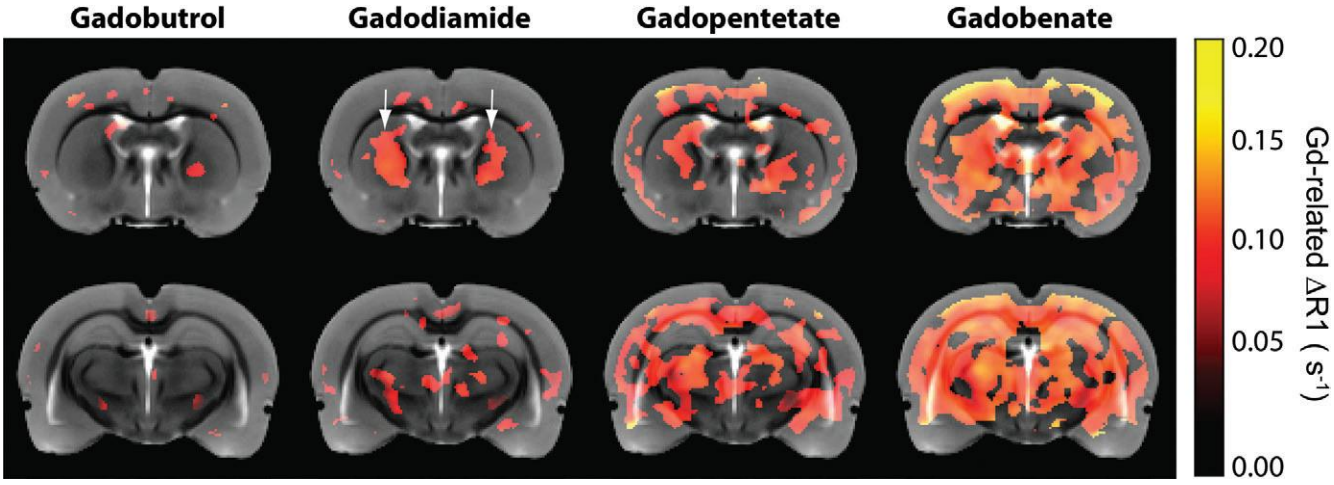

Figure 1: MRI templates show distribution of gadolinium-related longitudinal relaxation rate (R1) increases (ΔR1) in rats treated with gadobutrol, gadodiamide, gadopentetate, or gadobenate. ΔR1 for each gadolinium-treated group was compared with a saline-injected control group in a voxel-by-voxel manner. Voxels with ΔR1, which are significantly different ($P < .05$) from that of the saline group (color maps), were defined as gadolinium-related ΔR1 voxels. The corresponding ΔR1 values were overlaid on a T2-weighted MRI template (gray images). Arrows point to bilateral gadolinium-related ΔR1 in caudate-putamen in rats treated with gadodiamide.

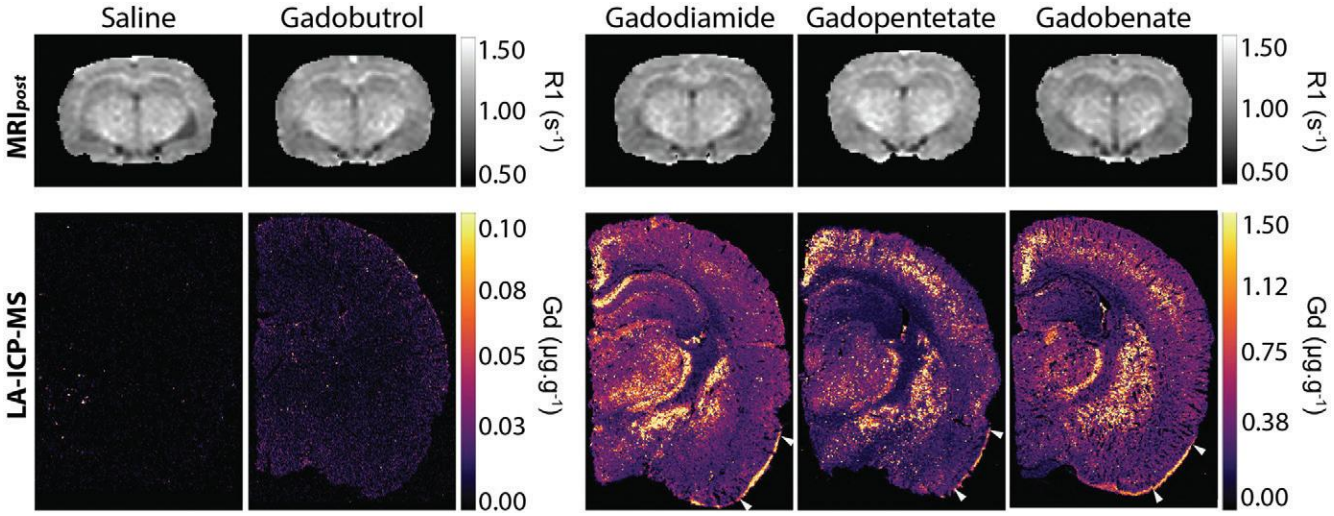

Figure 2: Representative longitudinal relaxation rate (R1) maps 1 week after the final (fifth) intravenous injection of gadolinium (Gd)–based contrast agent (GBCA) or saline (top row, both hemispheres) and corresponding laser ablation inductively coupled plasma mass spectrometry (LA-ICP-MS) brain maps of retained gadolinium (bottom row, left hemisphere) at the level of the rostral hippocampus. Arrowheads denote dorsal and ventral extent of layer 1 in the piriform cortex. MRI_{post} = MRI scan acquired at the time point of 1 week after the final injection of GBCA or saline.

gadolinium-related ΔR1 was observed in cerebral cortex, hippocampus, caudate-putamen, globus pallidus, and thalamus. Gadolinium-related ΔR1 was not observed in piriform cortex, amygdala, or hypothalamus.

In the gadopentetate group, 20.6% (0.38 of 1.86 cm^3) of brain volume showed gadolinium-related ΔR1, and in those regions, average ΔR1 was 0.069 $second^{-1}$ ± 0.018. Bilateral gadolinium-related ΔR1 in the gadopentetate group was detected in deep layers of the cerebral cortex, globus pallidus, and medial caudate-putamen with notable sparing of hippocampus and ventral thalamus.

In the gadodiamide group, there were gadolinium-related R1 increases in 5.4% (0.10 of 1.86 cm^3) of brain volume, and in those regions, average ΔR1 was 0.055 $second^{-1}$ ± 0.019. Gadolinium-related ΔR1 showed bilateral changes in the caudate-putamen.

In the gadobutrol group, 2.2% (0.04 of 1.86 cm^3) of brain volume showed gadolinium-related R1 increases, and in those regions, average ΔR1 was 0.052 $second^{-1}$ ± 0.041. We did not detect region-specific bilateral ΔR1 in the forebrain of rats treated with gadobutrol.

Collectively, MRI R1 mapping revealed agent-specific variation in the distribution of gadolinium-related ΔR1 in the brain of rats treated with gadobenate, gadopentetate, gadodiamide, or gadobutrol.

Gadolinium Retention in Rat Brain Evaluated with Postmortem LA-ICP-MS Elemental Mapping

Representative gadolinium brain i maps generated by quantitative LA-ICP-MS elemental analysis are shown in Figures 2 and 3. Rats treated with gadodiamide, gadopentetate, gado-

benate, or gadobutrol exhibited average concentrations of retained gadolinium in the forebrain at 0.60 μg · g^{-1} ± 0.11, 0.50 μg · g^{-1} ± 0.10, 0.45 μg · g^{-1} ± 0.07, or 0.01 μg · g^{-1} ± 0.00, respectively (Fig 3). The concentrations of retained gadolinium in rats treated with GBCAs were significantly greater compared with saline controls (P < .001 for all four groups). In addition, the average gadolinium concentrations in rats treated with gadodiamide, gadopentetate, or gadobenate were significantly greater compared with rats treated with gadobutrol (all P < .001). We also found that the average gadolinium concentration in rats treated with gadodiamide was significantly greater than in rats treated with gadobenate (P < .01) but not gadopentetate (P = .15).

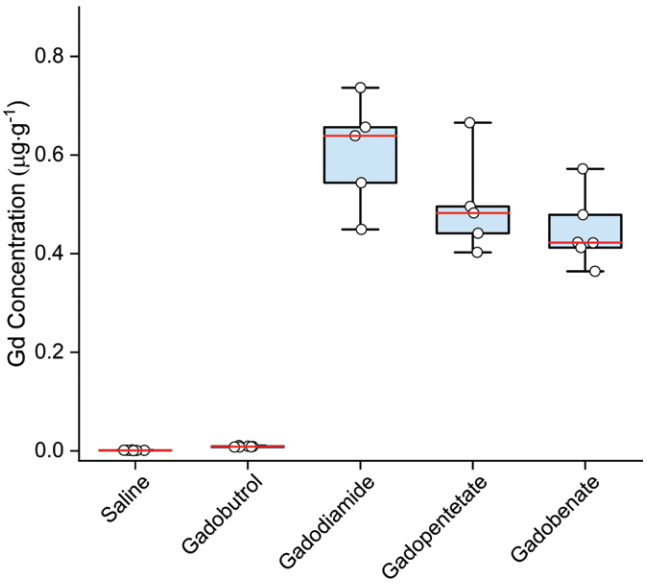

Figure 3: Box and whisker plot shows the average gadolinium (Gd) concentration measured with laser ablation inductively coupled plasma mass spectrometry at the level of the rostral hippocampus in rat brains 1 week after the final (fifth) intravenous injection of one of four gadolinium-based contrast agents (GBCAs) or saline. The average gadolinium concentration for individual rats is indicated by small circles in the box and whisker plot for each treatment condition. The red line indicates the median, and the box indicates the first and third quartiles. The average gadolinium concentrations in all GBCA groups were significantly greater compared with the saline control group (P < .001). Average gadolinium concentrations in rats treated with gadodiamide, gadopentetate, or gadobenate were significantly greater than that with gadobutrol (all P < .001). Average gadolinium concentrations in rats treated with gadodiamide were significantly greater than that with gadobenate (P < .01).

Next, we performed region-of-interest analysis of forebrain gadolinium distribution in GBCA- versus saline-treated rats. Intraclass correlation coefficient for regions of interest assessed by two independent readers showed excellent reliability (0.93; 95% CI: 0.88, 0.96). In contrast to MRI R1 results, regional LA-ICP-MS showed that rats treated with gadodiamide, gadopentetate, or gadobenate exhibited similar patterns of regional gadolinium retention in cerebral cortex and subcortical nuclei, including anterior cingulate cortex, piriform cortex, hippocampus (cornu ammonis), dentate gyrus, caudate-putamen, globus pallidus, and thalamic nuclei (Fig 2, Table 2). We detected layer-specific gadolinium retention (Figs 2, 4). For example, primary somatosensory cortex showed laminar gadolinium retention with predominance in middle cortical layers in rats treated with gadodiamide, gadopentetate, or gadobenate (Fig 4). All three GBCAs exhibited peak gadolinium retention at approximately 60% of the relative cortical depth. Layer-specific gadolinium retention was also detected in the anterior cingulate cortex and piriform cortex in rats treated with gadodiamide, gadopentetate, or gadobenate (Fig 2). In these three GBCA-treated groups, retained gadolinium was also detected in the choroid plexus (Fig 2, Table 2). Low-level gadolinium retention was detected in white matter (internal capsule) (Fig 2, Table 2). Rats treated with gadobutrol showed low levels of gadolinium retention in the forebrain and choroid plexus, a vascular endothelial tissue in the ventricles (Fig 2, Table 2).

Comparison of MRI and LA-ICP-MS Measures of Gadolinium Retention in Brain

The relaxation rate $R1_{post}$ measured 1 week after the final (fifth) GBCA administration provides a snapshot metric of gadolinium retention derived from quantitative MRI. We observed differences between measures of gadolinium retention measured with quantitative MRI ($R1_{post}$) and LA-ICP-MS elemental mapping (Fig 2). ΔR1 maps (Fig 1) showed partial concordance with gadolinium LA-ICP-MS mapping results (Fig 2). In rats treated with gadopen-

Table 2: Mean Gadolinium Concentration Measured with Laser Ablation Inductively Coupled Plasma Mass Spectrometry in Discrete Regions of the Brain

Brain Region	Gadobutrol	Gadodiamide	Gadopentetate	Gadobenate
Anterior cingulate cortex (layers 2 and 3)	0.01 ± 0.00	0.95 ± 0.18	0.92 ± 0.15	0.91 ± 0.11
Piriform cortex (layer 1)	0.01 ± 0.00	0.88 ± 0.07	0.74 ± 0.16	0.42 ± 0.03
Hippocampus (stratum pyramidale, *CA1*)	0.01 ± 0.00	0.77 ± 0.20	0.57 ± 0.18	0.40 ± 0.07
Dentate gyrus	0.01 ± 0.00	0.51 ± 0.08	0.37 ± 0.04	0.35 ± 0.03
Caudate-putamen	0.01 ± 0.00	1.07 ± 0.17	0.77 ± 0.08	0.66 ± 0.06
Thalamus (lateral dorsal nucleus)	0.01 ± 0.00	0.57 ± 0.07	0.47 ± 0.09	0.44 ± 0.04
Thalamus (reticular nucleus)	0.01 ± 0.00	1.14 ± 0.09	0.91 ± 0.10	0.96 ± 0.09
Globus pallidus (lateral subdivision)	0.01 ± 0.00	1.72 ± 0.30	1.21 ± 0.25	1.37 ± 0.09
Internal capsule (white matter)	0.01 ± 0.00	0.25 ± 0.02	0.24 ± 0.03	0.23 ± 0.02
Choroid plexus (ventricular)	0.08 ± 0.02	2.50 ± 0.21	1.54 ± 0.37	1.91 ± 0.52

Note.—Values represent means ± standard errors of means (gadolinium, in μg · g^{-1}). CA1 = cornu Ammonis 1.

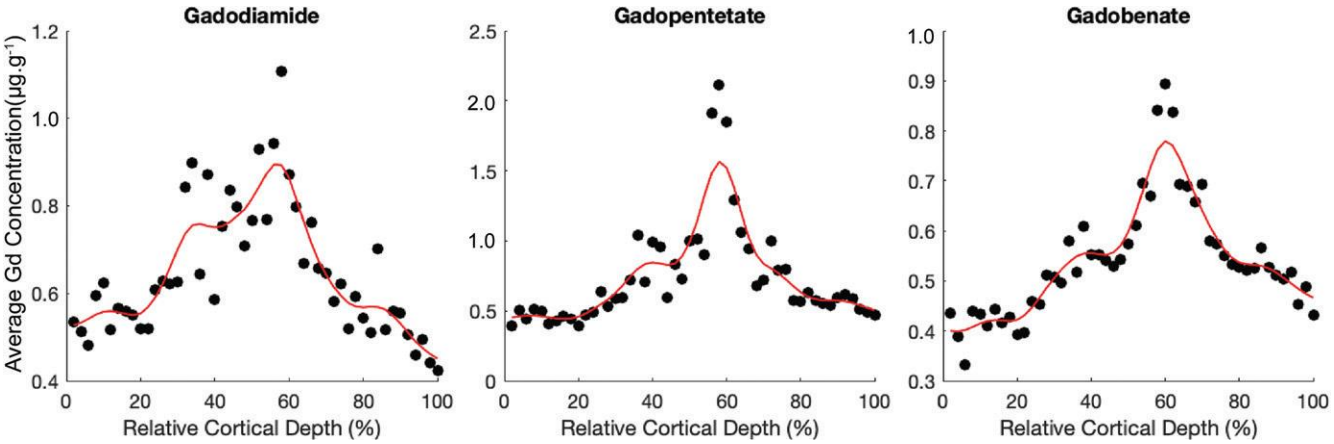

Figure 4: Dotted line graphs show the nonhomogeneous laminar distribution of retained gadolinium (Gd) detected with laser ablation inductively coupled plasma mass spectrometry elemental mapping in the primary somatosensory cortex (barrel field) of the brains of rats treated with a linear gadolinium-based contrast agent (GBCA) (gadodiamide, gadopentetate, or gadobenate). The line profiles of gadolinium concentration in the primary somatosensory cortex were measured along an axis line drawn perpendicular to the cortical surface to the underlying white matter (external capsule). Line length was normalized to cortical thickness to obtain relative cortical depth. Values were averaged for each GBCA group at the same relative cortical depth (dots) and plotted as a smoothed average profile (red line).

tetate or gadobenate, we observed gadolinium-related R1 increases in cerebral cortex, globus pallidus, and caudate-putamen that partially accord with regional gadolinium retention detected with LA-ICP-MS. However, gadolinium-related ΔR1 was detected in hippocampus and ventral thalamus in rats treated with gadobenate but not gadopentetate (Fig 1), which is discordant with LA-ICP-MS mapping results (Fig 2) that show similar patterns of retained gadolinium after repeated treatment with either two GBCAs. Differences between R1 and LA-MS-ICP maps were most notable in the gadodiamide treatment group. MRI R1 mapping revealed bilateral gadolinium-related ΔR1 (Fig 1) in the caudate-putamen of gadodiamide-treated rats. By contrast, LA-ICP-MS brain mapping in rats treated with gadodiamide showed a regional gadolinium distribution pattern that was similar to that in rats treated with gadopentetate or gadobenate (Fig 2, Table 2). Differences between MRI and LA-ICP-MS measures of gadolinium retention were also notable in piriform cortex where gadolinium retention in rats treated with gadopentetate, gadobenate, or gadodiamide was detected with LA-ICP-MS mapping but not with MRI R1 mapping.

Discussion

MRI examinations with gadolinium-based contrast agents (GBCAs) are associated with gadolinium retention in the brain (4–13). However, the question of whether MRI results accurately reflect gadolinium concentrations and distribution in the brain remains unanswered. In this study, we found that rats administered one of three linear GBCAs showed different patterns of gadolinium retention detected with R1 MRI. Gadolinium-related R1 changes (ΔR1) in the rat brains were 0.087 second^{-1} ± 0.051 for rats administered gadobenate and 0.069 second^{-1} ± 0.018 and 0.055 second^{-1} ± 0.019 for rats administered gadopentetate and gadodiamide, respectively. This was also indicated by different percentages of brain volume showing gadolinium-related ΔR1 (39.5%, 20.6%, or 5.4%, respectively) in rats treated with gadobenate, gadopentetate, or gadodiamide. However, these three linear GBCAs showed similar patterns of gadolinium retention detected with laser ablation inductively coupled plasma mass spectrometry (LA-ICP-MS). R1 mapping results are discordant with findings of LA-ICP-MS mapping.

For example, gadolinium-related ΔR1 was observed in multiple forebrain regions in gadobenate- or gadopentetate-treated rats but only a limited number of brain regions (eg, caudate-putamen) in gadodiamide-treated rats. By contrast, LA-ICP-MS mapping revealed a similar regional pattern of retained gadolinium in rats treated with one of three linear class GBCAs (gadodiamide, gadopentetate, or gadobenate). Moreover, gadolinium retention was detected with LA-ICP-MS in discrete regions and subregions of the forebrain that were not observed with R1 MRI mapping. For example, LA-ICP-MS mapping revealed layer-specific gadolinium retention in piriform cortex in rats treated with linear class GBCAs that were not detected with MRI R1 mapping.

We ascribe the observed differences between MRI R1 and LA-ICP-MS measures of gadolinium retention in the brain to differences in the origin of signals detected with each modality. MRI R1 is proportional to the product of concentration and molar relaxivity of gadolinium-containing complexes (16), the latter of which is influenced by various confounding factors (16,27). For example, in a microenvironment containing biologically ubiquitous cations (eg, calcium, iron, zinc, copper), gadolinium may be released from its chelate through transmetalation (28–32) and bind to soluble and insoluble macromolecules by means of transchelation (33). Differences between R1 and LA-ICP-MS maps were most pronounced in rats treated with gadodiamide, followed by gadopentetate, and least with gadobenate. This rank order is consistent with GBCA thermodynamic instability (28,34). Soluble gadolinium-containing macromolecular complexes exhibit decreased molecular tumbling that approach the Larmor frequency of protons and increase molar relaxivity of gadolinium. Insoluble gadolinium-containing complexes have limited water accessibility, becoming MRI silent. The differences we observed between MRI R1 scans and

LA-ICP-MS suggest that specific pools of retained gadolinium may be stored as insoluble complexes that escape MRI detection. This finding is consistent with a prior report of electron-dense deposits of insoluble $GdPO_4$ in the brains from rats administered gadodiamide (35). Speciation analysis also suggests that gadolinium may be stored in insoluble macromolecular complexes in the rat brain following repeated administration of gadodiamide (12,33).

We also want to point out that the regional and laminar distribution of gadolinium retention detected with LA-ICP-MS in rats treated with linear GBCAs is colocalized with parenchymal iron, as we previously reported for gadopentetate (14). We speculate that colocalization of gadolinium retention and iron enrichment may reflect shared carriers, transporters, and trafficking mechanisms by which these metals cross the blood-brain barrier and distribute in the brain (14).

The study has several limitations. First, we used a mixed turbo spin-echo sequence that samples only two points on the nonlinear R1 relaxation curve. Results using this sequence may deviate from that obtained with inversion recovery–based sequences. Second, tissue processing may result in leaching of soluble gadolinium species that might lead to differential agent-specific extraction. This potential confound may contribute to low levels of retained gadolinium in gadobutrol-treated rats. We also cannot exclude possible confounding effects due to variation in extraction efficiency of different gadolinium complexes that cannot be distinguished with LA-ICP-MS. Third, our results may be biased by species, age, sex, and intersubject variation of the rat model, as well as by the high-dose GBCA regimen and single post-exposure interval of our study. Accordingly, our study does not address lower dose GBCA regimens or long-term gadolinium retention in the brain. Fourth, this study included a single macrocyclic GBCA (gadobutrol), thus limiting generalization across this class. Finally, we cannot rule out other potential confounds.

The results of this study underscore several important caveats regarding interpretation of MRI measures attributed to gadolinium retention in the brain. Attributing MRI measures such as T1-weighted hyperintensity or increased longitudinal relaxation rate (R1) to increased gadolinium tissue concentration may lead to an underestimation of localization or extent of gadolinium retention. More importantly, based on our laser ablation inductively coupled plasma mass spectrometry (LA-ICP-MS) results, the absence of T1-weighted hyperintensity or increased R1 does not preclude the presence of retained gadolinium in the brain. T1-weighted or R1 MRI measures do not provide sufficient information to make analytical assessments regarding local gadolinium tissue concentrations in the brain. In conclusion, our results indicate differences between in vivo R1 mapping MRI and ex vivo LA-ICP-MS imaging measures of gadolinium retention in the forebrain. Caution is warranted when interpreting MRI R1 maps with respect to gadolinium retention, concentration, and distribution in the brain. In particular, the absence of MRI manifestation may not rule out the possibility that the subjects are free from gadolinium deposition.

Acknowledgments: The authors acknowledge the use of resources and facilities at and support from the Center for Biomedical Imaging, Boston University School of Medicine (Boston, Mass). The authors acknowledge resource support from Thermo Scientific (Waltham, Mass) and Office of the Dean, Boston University School of Medicine.

Author contributions: Guarantor of integrity of entire study, **L.E.G.**; study concepts/study design or data acquisition or data analysis/interpretation, all authors; manuscript drafting or manuscript revision for important intellectual content, all authors; approval of final version of submitted manuscript, all authors; agrees to ensure any questions related to the work are appropriately resolved, all authors; literature research, **N.H., O.M., L.E.G.**; experimental studies, **N.H., O.M., N.L., E.S.F., X.L., J.A.M., K.J.B., H.J., L.E.G.**; statistical analysis, **N.H., O.M., Y.T.**; and manuscript editing, **N.H., O.M., J.A.M., H.J., A.G., J.A.S., S.W.A., L.E.G.**

Disclosures of conflicts of interest: **N.H.** No relevant relationships. **O.M.** No relevant relationships. **N.L.** No relevant relationships. **E.S.F.** No relevant relationships. **X.L.** No relevant relationships. **J.A.M.** No relevant relationships. **K.J.B.** No relevant relationships. **H.J.** Royalties from the book *Theory of Quantitative Magnetic Resonance Imaging*: World Scientific, 2013; named inventor for the following patents issued or pending for Boston University and/or Boston Medical Center: Jara H, Synthetic Images for an MRI scanner using linear combination of source images to generate contrast and spatial navigation, 2004 U.S. patent number US 6,823,205 B1; Jara H, Divisional I (Additional Methods) for Synthetic Images for an MRI scanner using linear combination of source images to generate contrast and spatial navigation. 2005 U.S. patent number US 6,917,199; Jara H, Divisional II (Devices) for Synthetic Images for an MRI scanner using linear combination of source images to generate contrast and spatial navigation. 2006 U.S. patent number US 7,002,345; Jara H, Mian A, Sakai O, et al. Aqueous contrast agents for dynamic MRI and MRA, PTC/US2015/030703, 2015; WO 2015/179196; Jara H, Multi-spectral MRI scan with magnetization recovery, 10/114,095, 2018 USPTO, USA; and Jara H, White Matter Fibrography by Synthetic Magnetic Resonance Imaging. US and International patent application 05-2019; associate editor for *Radiology*. **Y.T.** Grant: P30-AG072978; grants or contracts: R01AG061028, U01 NS093334, R01 ES027584, R01AG062348, R01 HD090191, R01 OH011511, R03 AG06325, U54NS115266. **A.G.** Consulting fees from Pfizer, AstraZeneca, TissueGene, MerckSerono, Regeneron, Novartis; stock from BICL; consultant for *Radiology*. **J.A.S.** No relevant relationships. **S.W.A.** No relevant relationships. **L.E.G.** No relevant relationships.

References

1. McDonald RJ, Levine D, Weinreb J, et al. Gadolinium Retention: A Research Roadmap from the 2018 NIH/ACR/RSNA Workshop on Gadolinium Chelates. Radiology 2018;289(2):517–534.
2. Hunt CH, Hartman RP, Hesley GK. Frequency and severity of adverse effects of iodinated and gadolinium contrast materials: retrospective review of 456,930 doses. AJR Am J Roentgenol 2009;193(4):1124–1127.
3. Behzadi AH, Zhao Y, Farooq Z, Prince MR. Immediate Allergic Reactions to Gadolinium-based Contrast Agents: A Systematic Review and Meta-Analysis. Radiology 2018;286(2):471–482.
4. Errante Y, Cirimele V, Mallio CA, Di Lazzaro V, Zobel BB, Quattrocchi CC. Progressive increase of T1 signal intensity of the dentate nucleus on unenhanced magnetic resonance images is associated with cumulative doses of intravenously administered gadodiamide in patients with normal renal function, suggesting dechelation. Invest Radiol 2014;49(10):685–690.
5. Kanda T, Fukusato T, Matsuda M, et al. Gadolinium-based Contrast Agent Accumulates in the Brain Even in Subjects without Severe Renal Dysfunction: Evaluation of Autopsy Brain Specimens with Inductively Coupled Plasma Mass Spectroscopy. Radiology 2015;276(1):228–232.
6. McDonald RJ, McDonald JS, Kallmes DF, et al. Intracranial Gadolinium Deposition after Contrast-enhanced MR Imaging. Radiology 2015;275(3):772–782.
7. Roberts DR, Holden KR. Progressive increase of T1 signal intensity in the dentate nucleus and globus pallidus on unenhanced T1-weighted MR images in the pediatric brain exposed to multiple doses of gadolinium contrast. Brain Dev 2016;38(3):331–336.
8. McDonald RJ, McDonald JS, Kallmes DF, et al. Gadolinium Deposition in Human Brain Tissues after Contrast-enhanced MR Imaging in Adult Patients without Intracranial Abnormalities. Radiology 2017;285(2):546–554.
9. Kanda T, Ishii K, Kawaguchi H, Kitajima K, Takenaka D. High signal intensity in the dentate nucleus and globus pallidus on unenhanced T1-weighted MR images: relationship with increasing cumulative dose of a gadolinium-based contrast material. Radiology 2014;270(3):834–841.

10. Robert P, Lehericy S, Grand S, et al. T1-Weighted Hypersignal in the Deep Cerebellar Nuclei After Repeated Administrations of Gadolinium-Based Contrast Agents in Healthy Rats: Difference Between Linear and Macrocyclic Agents. Invest Radiol 2015;50(8):473–480.
11. Lohrke J, Frisk AL, Frenzel T, et al. Histology and Gadolinium Distribution in the Rodent Brain After the Administration of Cumulative High Doses of Linear and Macrocyclic Gadolinium-Based Contrast Agents. Invest Radiol 2017;52(6):324–333.
12. Gianolio E, Bardini P, Arena F, Gadolinium Retention in the Rat Brain: Assessment of the Amounts of Insoluble Gadolinium-containing Species and Intact Gadolinium Complexes after Repeated Administration of Gadolinium-based Contrast Agents. Radiology 2017;285(3):839–849.
13. Robert P, Fingerhut S, Factor C, et al. One-year Retention of Gadolinium in the Brain: Comparison of Gadodiamide and Gadoterate Meglumine in a Rodent Model. Radiology 2018;288(2):424–433.
14. Minaeva O, Hua N, Franz ES, et al. Nonhomogeneous Gadolinium Retention in the Cerebral Cortex after Intravenous Administration of Gadolinium-based Contrast Agent in Rats and Humans. Radiology 2020;294(2):377–385.
15. Davies J, Marino M, Smith APL, et al. Repeat and single dose administration of gadodiamide to rats to investigate concentration and location of gadolinium and the cell ultrastructure. Sci Rep 2021;11(1):13950.
16. Caravan P, Ellison JJ, McMurry TJ, Lauffer RB. Gadolinium(III) Chelates as MRI Contrast Agents: Structure, Dynamics, and Applications. Chem Rev 1999;99(9):2293–2352.
17. Fingerhut S, Niehoff AC, Sperling M, et al. Spatially resolved quantification of gadolinium deposited in the brain of a patient treated with gadolinium-based contrast agents. J Trace Elem Med Biol 2018;45:125–130.
18. Fingerhut S, Sperling M, Holling M, et al. Gadolinium-based contrast agents induce gadolinium deposits in cerebral vessel walls, while the neuropil is not affected: an autopsy study. Acta Neuropathol (Berl) 2018;136(1):127–138.
19. Robert P, Frenzel T, Factor C, et al. Methodological Aspects for Preclinical Evaluation of Gadolinium Presence in Brain Tissue: Critical Appraisal and Suggestions for Harmonization-A Joint Initiative. Invest Radiol 2018;53(9):499–517.
20. Saito N, Sakai O, Ozonoff A, Jara H. Relaxo-volumetric multispectral quantitative magnetic resonance imaging of the brain over the human lifespan: global and regional aging patterns. Magn Reson Imaging 2009;27(7):895–906.
21. Kuno H, Jara H, Buch K, Qureshi MM, Chapman MN, Sakai O. Global and Regional Brain Assessment with Quantitative MR Imaging in Patients with Prior Exposure to Linear Gadolinium-based Contrast Agents. Radiology 2017;283(1):195–204.
22. Suzuki S, Sakai O, Jara H. Combined volumetric T1, T2 and secular-T2 quantitative MRI of the brain: age-related global changes (preliminary results). Magn Reson Imaging 2006;24(7):877–887.
23. Shan ZY, Yue GH, Liu JZ. Automated histogram-based brain segmentation in T1-weighted three-dimensional magnetic resonance head images. Neuroimage 2002;17(3):1587–1598.
24. Valdés-Hernández PA, Sumiyoshi A, Nonaka H, et al. An in vivo MRI template set for morphometry, tissue segmentation, and fMRI localization in rats. Front Neuroinform 2011;5:26.
25. Smith SM, Jenkinson M, Woolrich MW, et al. Advances in functional and structural MR image analysis and implementation as FSL. Neuroimage 2004;23(Suppl 1):S208–S219.
26. Paxinos G, Watson C. The Rat Brain in Stereotaxic Coordinates. 7th ed. London, England: Elsevier Academic Press, 2014.
27. Yang CT, Chuang KH. Gd(iii) chelates for MRI contrast agents: from high relaxivity to "smart", from blood pool to blood–brain barrier permeable. MedChemComm 2012;3(5):552–565.
28. Port M, Idée JM, Medina C, Robic C, Sabatou M, Corot C. Efficiency, thermodynamic and kinetic stability of marketed gadolinium chelates and their possible clinical consequences: a critical review. Biometals 2008;21(4):469–490.
29. Kimura J, Ishiguchi T, Matsuda J, et al. Human comparative study of zinc and copper excretion via urine after administration of magnetic resonance imaging contrast agents. Radiat Med 2005;23(5):322–326.
30. Idée JM, Port M, Raynal I, Schaefer M, Le Greneur S, Corot C. Clinical and biological consequences of transmetallation induced by contrast agents for magnetic resonance imaging: a review. Fundam Clin Pharmacol 2006;20(6):563–576.
31. Sarka L, Burai L, Brücher E. The rates of the exchange reactions between [Gd(DTPA)]2- and the endogenous ions Cu2+ and Zn2+: a kinetic model for the prediction of the in vivo stability of [Gd(DTPA)]2-, used as a contrast agent in magnetic resonance imaging. Chemistry 2000;6(4):719–724.
32. Rogosnitzky M, Branch S. Gadolinium-based contrast agent toxicity: a review of known and proposed mechanisms. Biometals 2016;29(3):365–376.
33. Frenzel T, Apte C, Jost G, Schöckel L, Lohrke J, Pietsch H. Quantification and Assessment of the Chemical Form of Residual Gadolinium in the Brain After Repeated Administration of Gadolinium-Based Contrast Agents: Comparative Study in Rats. Invest Radiol 2017;52(7):396–404.
34. Idée JM, Port M, Robic C, Medina C, Sabatou M, Corot C. Role of thermodynamic and kinetic parameters in gadolinium chelate stability. J Magn Reson Imaging 2009;30(6):1249–1258.
35. Rasschaert M, Schroeder JA, Wu TD, et al. Multimodal Imaging Study of Gadolinium Presence in Rat Cerebellum: Differences Between Gd Chelates, Presence in the Virchow-Robin Space, Association With Lipofuscin, and Hypotheses About Distribution Pathway. Invest Radiol 2018;53(9):518–528.